Journal of Directed Energy, **1**, Fall 2005, 219–232

Electric Discharge Pumped Oxygen–Iodine Laser Kinetics

Matthew Lange, Greg Pitz, Brian Smith, and Glen P. Perram*

Center for Directed Energy, Air Force Institute of Technology, 2950 Hobson Way, Wright–Patterson Air Force Base, Ohio 45433-7765

Chemical lasers offer the highest powers necessary for many weapons applications but require significant logistical support in the delivery of specialized fuels to the battlefield. The goal of a current multiuniversity research program is to demonstrate an oxygen–iodine laser with electrical discharge production of singlet oxygen. Typically, oxygen discharges are limited to about 15% yield for singlet oxygen. The electron excitation cross sections as a function of the ratio of the electric field vs. the number density of particles (E/N) are well established. However, the kinetics for electron and singlet oxygen interactions is considerably more difficult to study. Optical diagnostics for $O_2(a, b)$ and O have been applied to a double-microwave discharge flow tube. By examining the difference in singlet oxygen kinetics between the two discharges in series, considerable information regarding the excited-state, excited-state interactions is obtained. Under certain discharge conditions, the $O_2(a)$ concentration significantly increases outside of the discharge, even after thermal effects are accounted for. Unfortunately, the sensitivity of singlet oxygen yields from a microwave discharge to the initial excited oxygen inlet conditions is low, suggesting a kinetic limitation to generator performance.

KEYWORDS: Oxygen discharge kinetics, Oxygen iodine laser, Rotational Temperature, Singlet oxygen, Spectroscopy

1. Introduction

Chemical lasers offer the highest powers required for many weapons applications. Indeed, megawatt-class chemical laser devices have been available since the early 1980's.[2] The five highest-power lasers, hydrogen fluoride (HF), HF-overtone, deuterium fluoride (DF), oxygen–iodine (COIL), and carbon dioxide (CO_2), all employ gas phase gain media. Gas phase lasers have the strong advantage of rejecting heat by flowing the gases out of the resonator. Furthermore, chemical lasers offer high output power per total system weight, critical for deploying these devices on mobile military platforms. Finally, the shorter wavelengths, particularly for COIL and HF-overtone, provide greater brightness on target for the same device power. With these advantages, chemical lasers have become the heart of current laser weapon development programs, including the Mobile Tactical High Energy Laser (MTHEL), Airborne Laser (ABL), and the Advanced Tactical Laser (ATL).

However, chemical lasers suffer from the limited magazine depth and logistical issues associated with novel fuels. The cost of delivering jet fuel to the battlefield now

Received November 4, 2004; revision received February 21, 2005.

*Corresponding author; e-mail: glen.perram@afit.edu.

exceeds the purchase price by an order of magnitude. Cost and complexity of using new, hazardous fuels will certainly affect the initial utility of these laser weapon systems. Thus, electrically driven lasers are perceived as highly desirable. The potential penalty in thermal management, degraded beam quality, and increased weight of electrically driven lasers may be acceptable particularly for lower-power (~100-kW), tactical missions. While diode pumped solid state lasers offer great promise in this arena, electrically driven gas phase (or liquid) lasers operating at short wavelengths may prove a viable alternative. The electric discharge pumped oxygen–iodine laser (ElectriCOIL)[3] is one such candidate.

The ElectriCOIL device offers a number of distinct advantages over standard COIL systems: 1) it eliminates the chlorine gas–liquid hydrogen peroxide singlet oxygen generator, 2) it offers the potential for closed cycle operation, 3) it capitalizes on recent advances in aircraft electrical power generation to produce large laser weapon magazine depth, 4) it utilizes the significant technology development associated with oxygen–iodine lasers, and 5) it retains the thermal management and beam quality advantages of gas phase gain media. Recently, gain has been demonstrated in a radio frequency (RF) discharge pumped oxygen iodine laser, in which atomic oxygen concentrations are limited by the addition of nitric oxide.[4]

In the ElectriCOIL device, the metastable energy carrier singlet oxygen, $O_2(a^1\Delta)$, is generated in a microwave or RF discharge. The fraction of molecular oxygen in this excited state is critical to the performance of the oxygen–iodine laser,[20] and the yield of singlet oxygen is often defined as the ratio of $O_2(a)$ concentration to total oxygen concentration. Yields of 11–32% have been reported in microwave, RF, and controlled-avalanche discharges.[1,6,9,17,18] Absolute concentrations of $O_2(a)$ are difficult to determine and are often in error by as much as 30–50%. This uncertainty contributes significantly to the range of reported yields. Note that the threshold yield for lasing at room temperature is about 15% (Ref. 20).

The objective of the present paper is to characterize the kinetics that limit the yield of singlet oxygen in a microwave discharge. In particular, the effects of introducing singlet molecular oxygen and ground-state oxygen atoms into the entrance of the discharge is studied in a double-discharge apparatus.

2. Laser Device Background

2.1. Chemical oxygen–iodine laser

The Chemical Oxygen–Iodine Laser (COIL) was first demonstrated at the Air Force Weapons Laboratory in 1977.[12] The first electronically excited state of molecular oxygen, $O_2(a)$, is produced by a two-phase reaction of chlorine gas and liquid basic hydrogen peroxide (BHP) with 40–60% efficiency.[20] Once produced, this singlet state of oxygen can be transported for considerable distances even at moderately high pressures, as the radiative lifetime is ~64 min and $O_2(a)$ is very resistant to collisional deactivation.[14] Thus, $O_2(a)$ is a metastable energy reservoir. Energy densities of 10–20 kJ/m^3 are typically attained. However, the long radiative lifetime leads to exceptionally low gain, and direct lasing on the $O_2(a^1\Delta–X^3\Sigma)$ magnetic dipole transition is not achievable.

Water is created as a byproduct of the chlorine–BHP reaction and entrained in the flow. Total conversion of chlorine to oxygen is not achieved in practice, with greater than 90%

chlorine utilization characteristic of well performing lasers. Molecular iodine is injected into the primary oxygen flow and is dissociated to atomic iodine by way of a complicated, poorly understood mechanism.[8] The average number of $O_2(a)$ molecules required to dissociate I_2, n, is highly variable, depending on water vapor concentration and other device-specific parameters, but must be greater than 2 and is typically ~5 (Ref. 20). The I_2 concentration is typically a small fraction (~1%) of the $O_2(a)$ concentration, and a single iodine atom is cycled many times through the energy transfer from singlet oxygen and subsequent stimulated emission.

COIL operates on an inversion between the $5^2P_{1/2}$ and $5^2P_{3/2}$ spin-orbit split states of atomic iodine at a wavelength of 1.315 μm. A near resonance exists between $O_2(a)$ and $I(^2P_{1/2})$ with an energy difference of only 3.3 kJ/mol, and laser pumping is achieved by collisional energy transfer from the $O_2(a)$ metastable energy reservoir, as shown in Fig. 1.[15] The energy transfer is rapid, and a near equilibrium between the upper laser level, $I(^2P_{1/2})$, and $O_2(a)$ is quickly established:

$$O_2(a^1\Delta) + I(^2P_{3/2}) \leftrightarrow O_2(X^3\Sigma) + I(^2P_{1/2}). \tag{1}$$

The ratio of excited and ground-state atomic iodine concentrations is approximately determined by the equilibrium constant for reaction (1), $K_{eq} = 0.75\exp(402/T)$:

$$\frac{[I(^2P_{1/2})]}{[I(^2P_{3/2})]} = \frac{[O_2(a^1\Delta)]}{[O_2(X^3\Sigma)]} K_{eq}(T), \tag{2}$$

where the brackets indicate concentration of the indicated specie.

The atomic iodine $5^2P_{1/2} \rightarrow 5^2P_{3/2}$ lasing transition is composed of six hyperfine components, and the $5^2P_{1/2}$ $(F' = 3) \rightarrow 5^2P_{3/2}$ $(F'' = 4)$ component provides the highest gain.

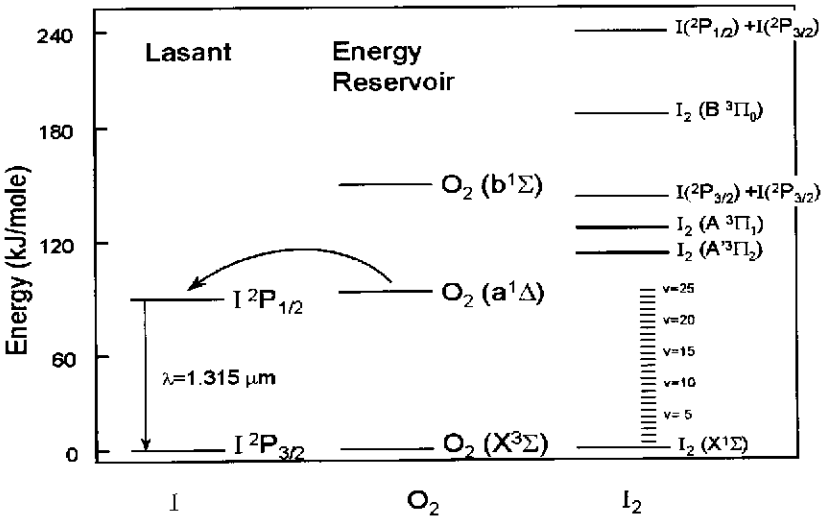

Fig. 1. Energy level diagram for COIL illustrating the resonant energy transfer from metastable reservoir $O_2(a^1\Delta)$ to the upper laser level of atomic iodine, $I(^2P_{1/2})$. The energy levels for several key states involved in the dissociation of molecular iodine are also provided.

The hyperfine levels are populated statistically, and the population inversion is

$$\Delta = \left[I(^2P_{1/2}, F' = 3)\right] - \left(\frac{g_2}{g_1}\right)\left[I(^2P_{3/2}, F'' = 4)\right]$$
$$= \left(\frac{7}{12}\right)\left(\left[I(^2P_{1/2})\right] - 0.5\left[I(^2P_{3/2})\right]\right) = \left(\frac{7}{12}\right)\left\{K_{eq}\left(\frac{Y}{1-Y}\right) - \frac{1}{2}\right\}\left[I(^2P_{3/2})\right], \quad (3)$$

where

$$Y = \text{yield} = \frac{\left[O_2(a^1\Delta)\right]}{\left[O_2(X^3\Sigma)\right] + \left[O_2(a^1\Delta)\right]}. \quad (4)$$

Threshold for lasing (positive inversion) is achieved at $T = 295$ K when the ratio of $O_2(a)$ to total oxygen, or yield of singlet oxygen, is approximately 15%. The threshold is reduced considerably at lower temperatures due to the temperature dependence of the equilibrium constant. At $T = 160$ K, a temperature consistent with typical nozzle exit conditions, the threshold yield is reduced to 5%. The cross section for stimulated emission at room temperature is $\sigma = 7.4 \times 10^{-18}$ cm^2 (4) and the gain in a COIL device is typically near $\gamma = 0.8\%$/cm.

The singlet oxygen yield in the plenum required to reach threshold is somewhat modified by the requirements to dissociate molecular iodine. Defining the yield consumed in the dissociation process from the I_2 and O_2 flow rates as

$$Y_{diss} = n\frac{\dot{n}_{I_2}}{\dot{n}_{O_2}}, \quad (5)$$

the resulting temperature dependent threshold yield is

$$Y_{th} = \frac{1}{1 + 2K_{eq}(T)} + Y_{diss}. \quad (6)$$

A plot of the threshold yield as a function of temperature is shown in Fig. 2 for $Y_{diss} = 0.075$, representative of a typical supersonic COIL device. The temperature in the gain region is significantly reduced by the supersonic expansion. For isentropic flow, the temperature is defined by the nozzle Mach number, M:

$$T = T_o\left(1 + \frac{\gamma - 1}{2}M^2\right)^{-1}, \quad (7)$$

where γ is the ratio of specific heats, $\gamma = c_p/c_v$, and T_o is the stagnation temperature. A typical COIL devices uses an $M = 2$ nozzle and the plenum temperature is near $T = 300$ K, yielding $T = 167$ K in the laser cavity. The threshold yield is significantly reduced at these lower temperatures. The measured yield and temperature for the 40-kW RotoCOIL device developed in the mid-1980's is shown in Fig. 2.[21] The power in the flow available for lasing is proportional to the plenum yield above threshold and the total oxygen flow rate. Alternatively, the oxygen flow rate may be derived from the chlorine flow rate and chorine utilization.[20] For example, a $Y = 50\%$ plenum yield, $Y_{th} = 7.5\%$ yield consumed by dissociation, cavity temperature of $T = 167$ K, $U_{Cl_2} = 90\%$ chlorine utilization, and chlorine flow rate of $\dot{n}_{Cl_2} = 1.5$ mol/s provides an available power of about $P_a = 52$ kW:

$$P_a = \left(91\frac{\text{kJ}}{\text{mol}}\right)\dot{n}_{Cl_2}U_{Cl_2}(Y - Y_{th}). \quad (8)$$

The energy stored per $O_2(a)$ molecule is 0.98 eV/molecule or 91 kJ/mol.

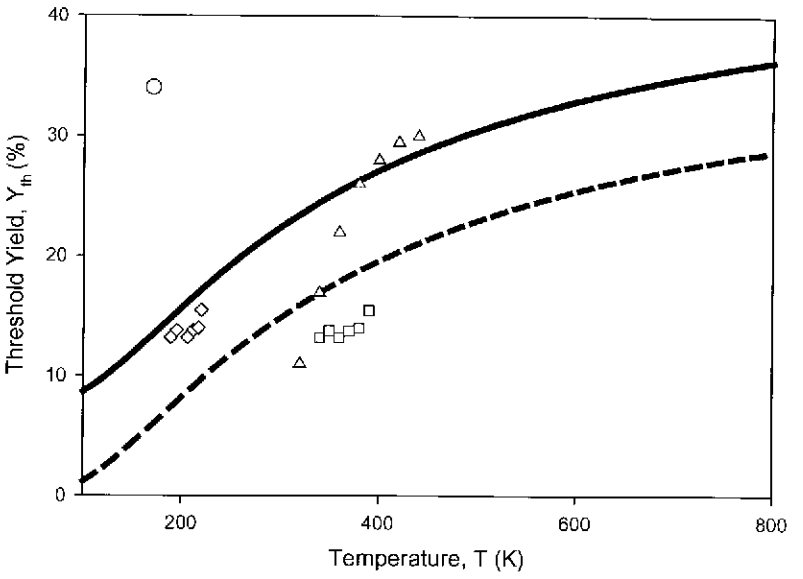

Fig. 2. Singlet oxygen yields: —, to reach threshold for $Y_{diss} = 7.5\%$; – –, to reach threshold for $Y_{diss} = 0\%$; ○, achieved in RotoCOIL device[20]; □, achieved by subsonic RF discharge[4]; ◇, RF yields at temperatures achievable with supersonic expansion; and △, modeled with He:O_2 = 4:1 (Ref. 4).

2.2. Electric discharge pumped oxygen–iodine laser (ElectriCOIL)

The discharge pumped oxygen–iodine laser exhibits a number of features in contrast to the COIL device: (1) the yield of singlet oxygen is lower, $Y \sim 15$–25%, (2) the stagnation temperature is higher, $T_o \sim 500$ K, (3) a large concentration of atomic oxygen exists, (4) no water vapor exists, and (5) the concentration of $O_2(b^1\Sigma)$ is significantly greater. Historically, the difficulty in developing an ElectriCOIL device is centered on the low yield of O_2(a) from self-sustained discharges. An insufficient fraction of the discharge power is partitioned into O_2(a) energy reservoir. The efficiency could be as high as 50% for a discharge with E/N δ 10 Td = 10^{-16} V-cm^2, where the cross section for excitation for the pumping reaction

$$e^- + O_2(X) \rightarrow e^- + O_2(a) \tag{9}$$

is maximized.[4] Unfortunately, stable discharges operate at 15–30 Td. Several approaches have been investigated to alter the discharge E/N realized, including electron beam sustainment, controlled avalanche discharges, and buffer gas (He, Ar, NO) addition.

The production of O_2(a, b) by plasma electrons is important in ionospheric chemistry, glow discharges for microelectronic processing, and the ElectriCOIL laser. Several kinetic models for such discharges exist.[5,11,19] These models must include several key elements: 1) electron excitation and deexcitation of singlet oxygen, 2) atomic oxygen production from direct electron impact and multiple-step dissociation from O_2^+ and excited O_2, 3) intermediate kinetics including O_2^+ and vibrationally excited O_2 production, and 4) collisional cascading to O_2(a) from O_2 states with energies of 1.5–5 eV (Ref. 5). A summary of some of these key reactions is provided in Table 1. The cross sections for electron interactions with ground-state molecular oxygen are rather well established and are shown in Fig. 3.[5,16]

Table 1. Key oxygen discharge kinetic processes

Reaction	Process	Rate coefficient, k_i (cm^3/particle-s)
9	$O_2 + e^- \rightarrow O_2(a) + e^-$	5×10^{-10}
9°	$O_2 + e^- \rightarrow O_2(b) + e^-$	—
10	$O_2(a) + e^- \rightarrow O_2 + e^-$	1.5×10^{-9}
11	$O_2(a) + e^- \rightarrow O + O + e^-$	$<1.4 \times 10^{-9}$
12	$O_2(a) + e^- \rightarrow O_2(b) + e^-$	—
13	$O_2 + e^- \rightarrow O + O + e^-$	9×10^{-9}
14	$O_2 + e^- \rightarrow O + O$	4×10^{-11}
15	$O_2 + e^- \rightarrow O_2^+ + e^- + e^-$	2×10^{-9}
16	$O_2^+ + e^- \rightarrow O + O$	2×10^{-7}

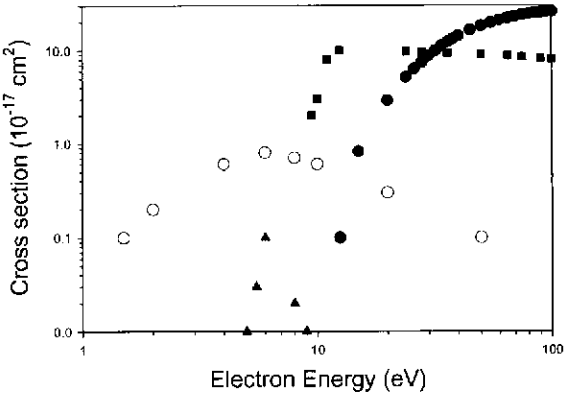

Fig. 3. Cross sections for molecular oxygen ●, ionization[16]; ○, excitation[5]; ■, dissociation[5]; and □, dissociative attachment.[5]

The rate coefficients depend on electron energy distributions, and the rates listed in Table 1 represent conditions typical of RF discharges.[5] Note that the dominant process in the electron energy range of importance (0–20 eV) is dissociation. Indeed, large atomic oxygen concentrations, as high as 40%, can be obtained.

As the singlet oxygen concentration increases, electron–excited state interaction becomes increasingly important. The yield of $O_2(a)$ is in part limited by superelastic collisions:

$$e^- + O_2(a^1\Delta) \rightarrow e^- + O_2(X^3\Sigma), \tag{10}$$

where the electron gains kinetic energy equivalent to the molecular oxygen internal excitation, and by dissociation of singlet oxygen,

$$e^- + O_2(a^1\Delta) \rightarrow e^- + O + O. \tag{11}$$

The rate for superelastic reaction (10) is constrained by detail balance and the rate for excitation reaction (9). The cross sections for dissociative reactions (11–14) and (16) are more difficult to measure and are not well established. In fact, the rate coefficient provided in Table 1 includes a significant contribution from vibrationally excited O_2.

In addition to the superelastic and dissociative removal of $O_2(a)$, excitation of $O_2(a)$ to higher electronic states, including $O_2(b)$, is possible. Indeed, the cross section for excitation of the $O_2(b)$ state from $O_2(a)$ of reaction (12) is an order of magnitude greater than the corresponding excitation from $O_2(X)$, reaction (9°). The cross section for reaction (12) at an electron energy of 4.5 eV is large, 23×10^{-18} cm^2 (Ref. 7), and comparable to the $O_2(a)$ production from reaction (9). In the traditional COIL, the concentration of $O_2(b)$ is small. However, in the ElectriCOIL concept, a significant $O_2(b)$ concentration is obtained. As much as 20% of the discharge electrical power results in $O_2(b)$ production.[10]

Recent oxygen discharge results are promising for ElectriCOIL development. In Fig. 2 the yields and temperatures recently achieved in a high-power RF discharge at the University of Illinois under subsonic conditions are above threshold after supersonic expansion. Furthermore, modeling suggests even better performance for a He:O_2 ratio of 4:1.

The discharge singlet oxygen generator produces large concentrations of atomic oxygen. Initially O atoms are helpful, as they assist in the dissociation of molecular iodine:

$$O + I_2 \rightarrow OI + I, \tag{17}$$

$$O + OI \rightarrow O_2(a) + I. \tag{18}$$

The rate for reactions (17) and (18) are very rapid, with rate coefficients of 1.4×10^{-10} and 1.5×10^{-10} cm^3/s, respectively.[13] Thus, the threshold yield is reduced to the value for $Y_{diss} = 0$. However, for O-atom concentrations greater than the I_2 concentration, there are deleterious effects, including the moderately fast quenching of $I(^2P_{1/2})$. The recent ElectriCOIL gain demonstration required the removal of excess atomic oxygen via the NO_2 titration reaction.[4]

3. Double-Discharge Experimental Apparatus

A two-element microwave discharge apparatus was developed to study the singlet oxygen kinetics, as shown in Fig. 4. The first discharge produces a flow of $O_2(a)$, $O_2(b)$, and atomic oxygen, as well as vibrationally excited states of oxygen, which then serve as the initial

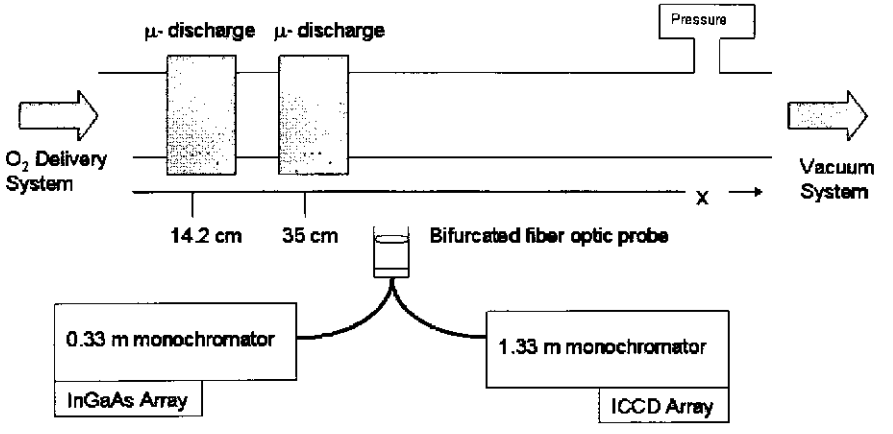

Fig. 4. Double microwave discharge flow tube with spectrally resolved emission diagnostics.

condition to the second discharge. The conditions can be changed by either varying the power of the first discharge or placing silver wool between the two discharges to control the O atom concentration. By looking into these changes and monitoring the output of the second discharge, one can determine the effects on the rates of electron and singlet oxygen interactions.

The ½ in. flow tube provides a typical flow velocity of 800 cm/s. Two similar Evenson-type microwave cavities with 120-W Opthos power supplies were employed to produce the oxygen discharges. The two discharges are separated by 20.8 cm, and optical access is largely obscured for 3 cm around each discharge. Pressure (3.8–4 torr) and flow rates (600–1000 sccm) were monitored with MKS 600-series capacitance manometers and Sierra capacitance-based flow controllers.

The principal diagnostics include both $O_2(a)$ and $O_2(b)$ spectra as a function of flow distance x. The optical emissions were collected with a fiber bundle and focusing probe providing approximately 0.5-cm spatial resolution in the flow direction. The $O_2(b)$ emission is resolved by a 1.3-m monochromator with ICCD camera detection, providing ~0.01-nm spectral resolution. The weaker $O_2(a)$ emission is resolved by a 0.3-m monochromator and an InGaAs array providing ~1.7-nm spectral resolution.

4. Double Microwave Discharge Results

4.1. Emission spectra and gas temperatures

The spectrally resolve emissions from $O_2(b^1\Sigma \rightarrow X^3\Sigma)$ near 762 nm and $O_2(a^1\Delta \rightarrow X^3\Sigma)$ near 1.27 μm are shown in Figs. 5 and 6. Nearly complete spectral isolation is achieved for the $O_2(b \rightarrow X)$ emission, allowing for clear determination of rotational population distributions. The rotational spectrum of the $O_2(b \rightarrow X)$ emission is labeled as ${}^{\Delta K}\Delta J(K'')$ where K is the total angular momentum without electron spin and J represents the total angular momentum (spin + rotation). The magnetic dipole selection rules, Hunds case (b), produces four branches: ${}^{P}P$ and ${}^{P}Q$, beginning near 1,320 cm^{-1} and extending to about 13,020 cm^{-1}, and the ${}^{R}Q$ and ${}^{R}R$ lines from 13,125 to 13,165 cm^{-1}.

The temperature of the discharged oxygen was monitored via the $O_2(b)$ rotational distribution

$$\frac{N(J)}{\sum_J N(J)} = \left(\frac{hcB}{kT}\right)(2J+1)e^{-F(J)hc/kT}, \tag{19}$$

where the concentration of a specific rotational state, $N(J)$, is related to the observed intensity through the rotational line strength, $S(J', J'')$ given in Table 2:

$$I(J) \propto N(J)S(J', J''), \tag{20}$$

Table 2. Rotational line strengths $S(J', J'')$, as a function of ΔK and ΔJ

	ΔK	ΔJ	$S_{J''}^{J'}$
${}^{R}R$	+1	+1	$\frac{1}{2}J''$
${}^{R}Q$	+1	0	$\frac{1}{2}(J''+0.25)$
${}^{P}P$	−1	−1	$\frac{1}{2}(J''+0.75)$
${}^{P}Q$	−1	0	$\frac{1}{2}(J''+1)$

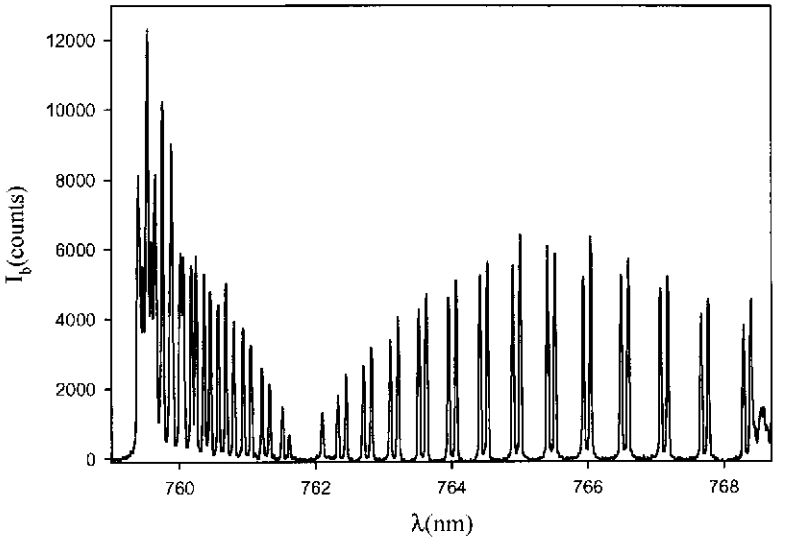

Fig. 5. Rotationally resolved $O_2(b^1\Sigma \rightarrow X^3\Sigma)$ emission spectrum observed from a microwave discharge operating at an oxygen pressure of 4.015 torr.

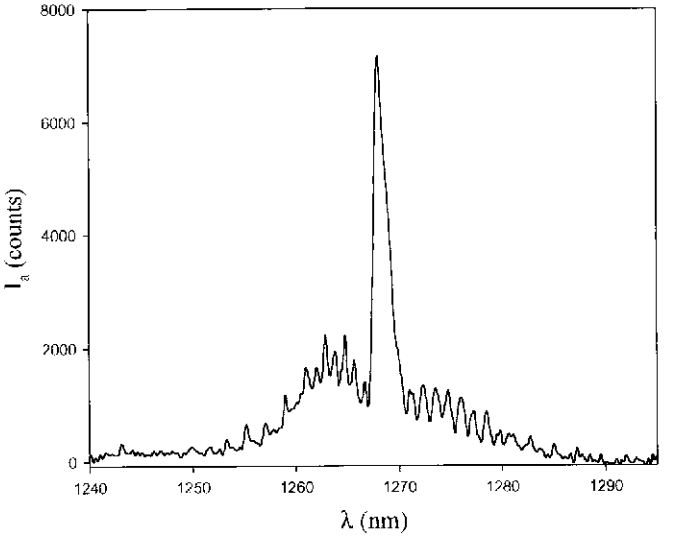

Fig. 6. Emission spectrum for $O_2(a^1\Delta - X^3\Sigma)$ $(v' = 0 \rightarrow v'' = 0)$ band recorded just after the second discharge at $x = 40.5$ cm for an oxygen pressure of 4.015 torr.

and the rotational state energies are specified by $F(J)$. A typical rotational population is provided in Fig. 7, illustrating a statistical distribution. Intensities are obtained from a fit to the area of a Gaussian lineshape. The error bounds in Fig. 7 represent the uncertainties in the fit areas. Both rotational branches yield a similar temperature, $T = 720 \pm 19$ and 721 ± 20 K. Observed temperatures range from 1,150 to 400 K, depending on discharge power and flow distance, x, as illustrated in Fig. 8.

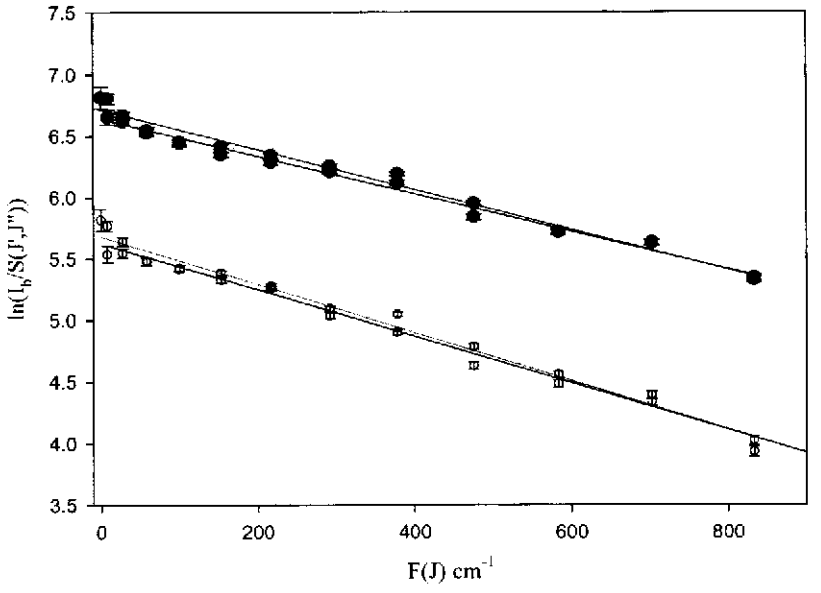

Fig. 7. Boltzmann distribution of ▲, △, ^{P}P and ●, ○, ^{P}Q branches for O_2(b) at ▲, ●, $x = 37.5$ cm and △, ○, $x = 40$ cm.

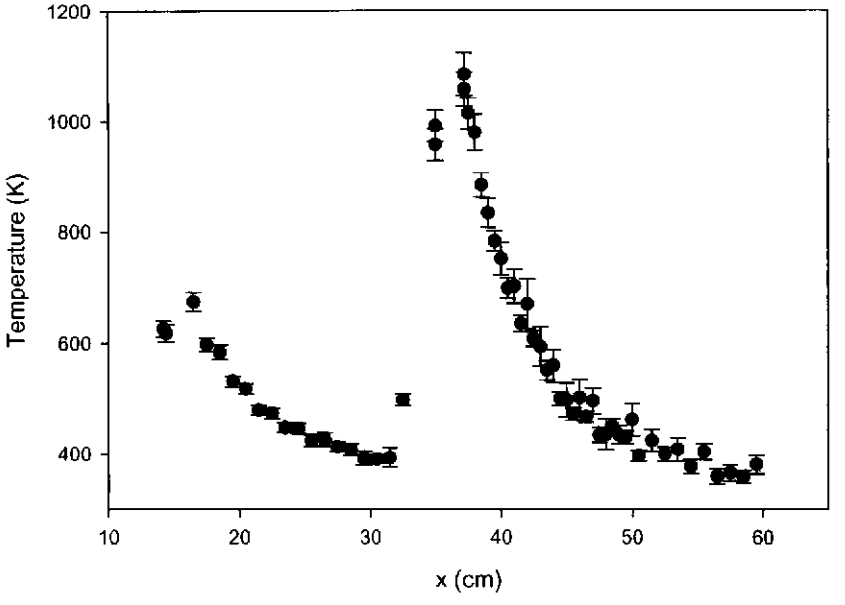

Fig. 8. Temperature as a function of flow distance with 85 W at $x = 14.2$ cm and 85 W at $x = 35$ cm and average oxygen pressure of 4.09 torr.

The significant temperature rise across the discharge directly affects the observed intensities. The emission intensities are proportional to the concentration of the emitter. However, pressure in the flow tube is nearly constant. Thus, any temperature increase produces a corresponding linear decrease in concentration and observed intensity. The $O_2(a \rightarrow X)$ emission

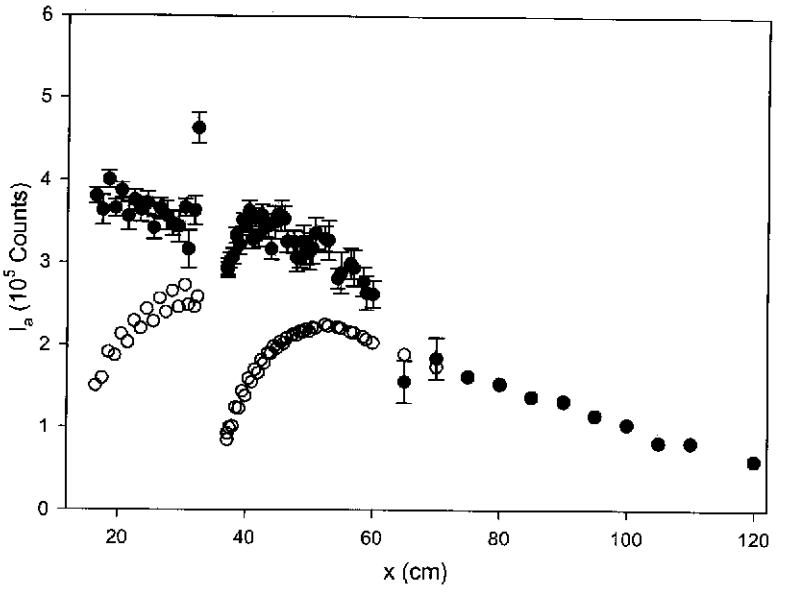

Fig. 9. Band-integrated intensity from $O_2(a \rightarrow X)$ emission as a function of flow tube distance: ○, as experimentally observed, and ●, corrected for temperature variation.

intensity, I_a, defined as the total area under the spectra, is shown as a function of distance along the flow tube in Fig. 9. The dramatic increase in intensity just outside of the discharge is largely attributed to the declining temperature. However, a definite increase (~28%) in $O_2(a)$ is observed even after the temperature change is accounted for. We are unaware of any previous reports of singlet oxygen production downstream of the discharge, and the source of this emission is under active investigation. Possible explanations include 1) relaxation to $O_2(a)$ from $O_2(b)$, or higher-lying oxygen electronic states; 2) vibrational relaxation from $O_2(a, v > 0)$; 3) atomic oxygen recombination; 4) ozone reactions; 5) thermal electron excitation; and 6) reactions involving $O(^1D)$.

4.2. Singlet oxygen kinetics

The flow tube kinetics of oxygen discharges have been studied extensively but almost always under conditions in which the $O_2(b)$ concentration is controlled by the pooling reaction

$$O_2(a) + O_2(a) \rightarrow O_2(b) + O_2(X) \tag{21}$$

with rate coefficient, $k_{21} = 2.7 \times 10^{-17}$ cm^3/molecule-s. For a total $O_2(b)$ deactivation decay rate of Γ_b, the steady-state concentration is

$$[O_2(b)] = \frac{k_{21}[O_2(a)]^2}{\Gamma_b}, \tag{22}$$

In Fig. 10, the $O_2(b)$ and $O_2(a)$ intensities are correlated. The steady-state relation of Eq. (22) is demonstrated by the linear portion of the plot at the lower $O_2(b)$ concentrations achieved at $x > 60$ cm. The steady-state conditions are largely unaffected by the

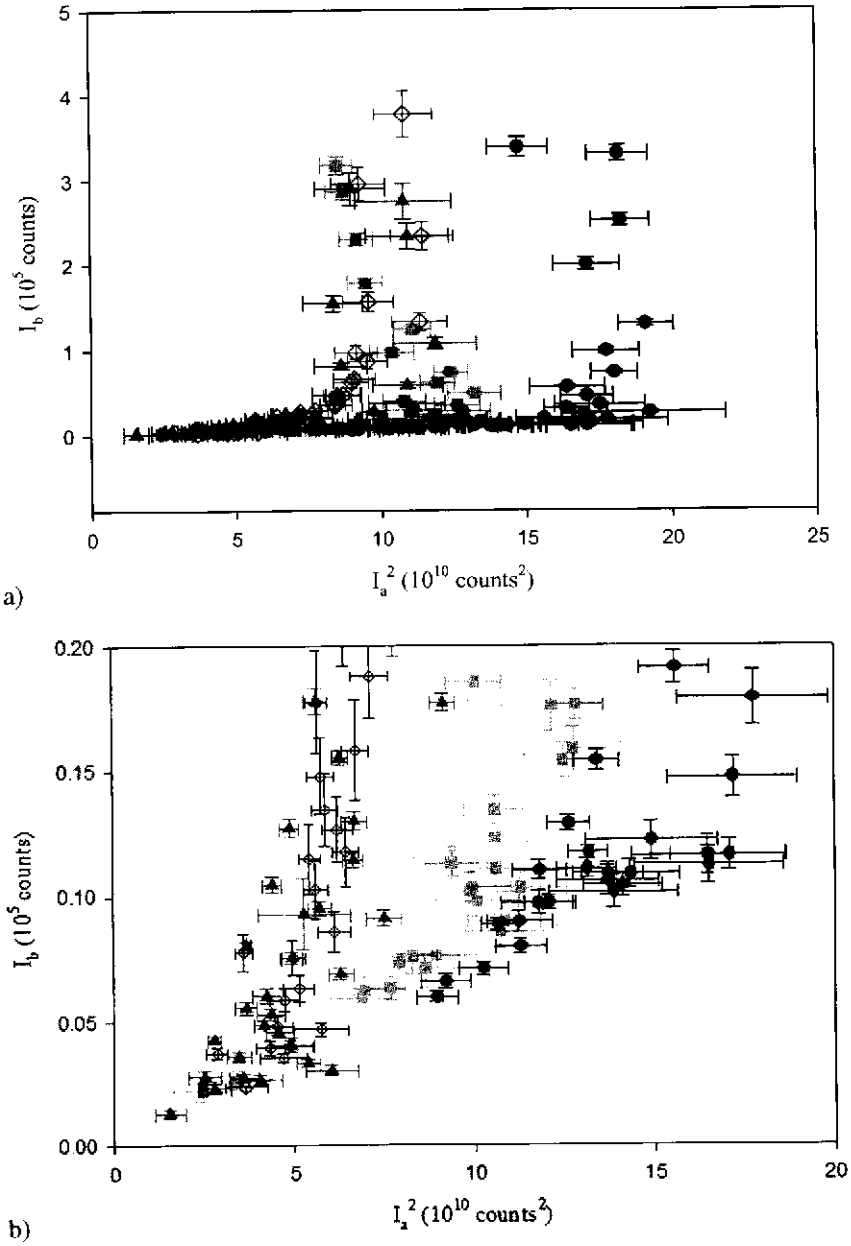

Fig. 10. Emission intensities from O_2(a) and O_2(b) for discharge powers of ■, 100–85 W; ●, 85–85 W; ▲, 70–70 W; and ◇, 0–85 W. In panel b the scale is expanded to illustrate steady-state O_2(b) concentrations.

injection of excited oxygen into the discharge. A significant deviation from these conditions is observed just outside the discharge where the O_2(b) concentration is much higher and, when excited oxygen is introduced to the second discharge, the O_2(a) concentration increases.

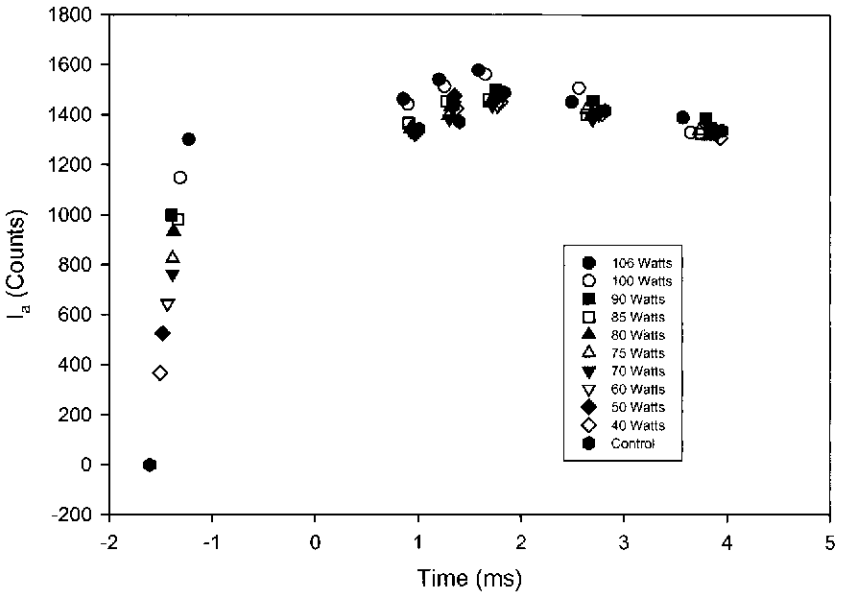

Fig. 11. Singlet-delta intensity before and after the second discharge ($x = 65$ cm) for a second discharge power of 82 W and first discharge power ranging from 40 to 100 W.

The $O_2(a)$ concentration at the exit of the second discharge depends only weakly on the power of the first discharge, as shown in Fig. 11. As the first discharge power is increased, a significant increase in $O_2(a)$, and presumably O and $O_2(X, v \gg 0)$, is delivered to the second discharge. However, only a small increase (5–8%) in $O_2(a)$ at the exit of the second discharge is observed. The discharge is relatively insensitive to inlet conditions, suggesting that a steady-state balance between production and destruction of singlet oxygen within the discharge is achieved at the flow rates employed in the current study. It is likely that a decrease in flow velocity, allowing for more energy deposition during the gas residence time, would yield little improvement in the yield of $O_2(a)$.

5. Conclusions

The singlet oxygen, $O_2(a, b)$, produced in a microwave discharge of pure molecular oxygen at modest flow rates provides an initial $O_2(b)$ concentration that exceeds the steady-state concentration controlled by pooling by more than a factor of 10, reflecting significant discharge yields. When singlet molecular oxygen and atomic oxygen are introduced to the inlet of the discharge, an increase in $O_2(a)$ is observed immediately outside of the discharge. The kinetic mechanism responsible for this production requires further study. If this production arises from relaxation from higher-lying states, then a significant increase in singlet oxygen yield may be obtained if a selective relaxation collision partner were identified. Unfortunately, the sensitivity of singlet oxygen yields from a microwave discharge to the initial excited oxygen inlet conditions is low, suggesting a kinetic limitation to generator performance. Indeed, the production of $O_2(a, b)$ is likely countered by second-order reactions whose rates increase as the singlet oxygen yield increases. In particular, the electron dissociation of $O_2(a, b)$ may be a critical limiting process. Uncovering this

limitation is critical to assessing the efficiency and scalability of the proposed ElectriCOIL device.

References

[1]Bernard, D.J., and N.R. Pchelkin, Rev. Sci. Instrum. **49**, 749 (1978).

[2]Bloembergen, N., and C.K.N. Patel (eds.), Rev. Mod. Phys. **59**, Part II (1987).

[3]Carroll, D.L., and W.C. Solomon, Proc. SPIE **4184**, 40 (2000).

[4]Carroll, D.L., J.T. Verdeyen, D.M. King, J.W. Zimmerman, J.K. Laystrom, B.S. Woodard, N. Richardson, K. Kittell, Mark J. Kushner, and W. C. Solomon, Appl. Phys. Lett. **85**, 1320 (2004).

[5]Dai, X.J., Aust. J. Phys. **49**, 1169 (1996).

[6]Fujii, H., "COIL in Japan," AIAA Paper 2000-2424 (2000).

[7]Hall, R.I., and S. Trajmar, J. Phys. B **8**, L293 (1975).

[8]Heaven, M.C., A.V. Komissarov, and V. Goncharov, Proc. SPIE **4631**, 13 (2002).

[9]Hill, A.E., *Proceedings of the International Conference on Lasers 2000*, 249, STS Press, McLean, VA (2001).

[10]King, D.M., D.L. Carroll, J.K. Laystrom, J.T. Verdeyen, M.S. Sexauer, and W.C. Solomon, *Proceedings of the International Conference on Lasers 2000*, STS Press, McLean, VA (2001).

[11]Lee, C., D.B. Graves, M.A. Lieberman, and D.W. Hess, J. Electrochem. Soc. **141** 1546 (1994).

[12]McDermott, W.E., N.R. Pchelkin, D.J. Benard, and R.R. Bousek, Appl. Phys. Lett. **32** 469 (1978).

[13]Payne, W.A., R.P. Thorn, Jr., F.L. Nesbitt, and L.J. Stief, J. Phys. Chem. A **102**, 6247 (1998).

[14]Perram, G.P., Int. J. Chem. Kinet. **27**, 817 (1995).

[15]Perram, G.P., Chemical Lasers, in J.G. Webster (ed.), *Wiley Encyclopedia of Electrical and Electronic Engineering*, Vol. 3, pp. 275–285, Wiley, New York (1999).

[16]Rapp, D., and P. Englander-Golden, J. Chem. Phys. **43**, 1464 (1965).

[17]Savin, Y.V., L.V. Goryachev, A.A. Adamenkov, Y.A. Adamenkov, V.V. Bakshin, V.V. Buzoverya, B.A. Vyskubenko, V.V. Yegorov, S.P. Ilyin, Y.V. Kolobyanin, and E.A. Kudryashov, Proc. SPIE **5120**, 433 (2003).

[18]Schmiedberger, J., S. Hirahara, Y. Ichinoche, M. Suzuki, W. Masuda, Y. Kihara, E. Yoshotani, and H. Fujii, Proc. SPIE **4184**, 32 (2001).

[19]Stafford, D.S., and M. J. Kushner, J. Appl. Phys. **96**, 2451 (2004).

[20]Truesdell, K.A., C.A. Helms, S. Frerking, and G.D. Hager, Proc. SPIE **3092**, 676 (1997).

[21]Truesell, K.A., C.A. Helms, and G.D. Hager, Proc. SPIE **2502**, 217 (1995).

The Authors

Mr. Matthew Lange received his B.S. degree in Physics from the University of Akron in 1999 and his M.S. degree in Applied Physics from the Air Force Institute of Technology in 2001. He is currently working to attain his Ph.D. degree in Applied Physics at the Air Force Institute of Technology.

Dr. Glen P. Perram received his B.S. degree in Applied Physics from Cornell University in 1980 and his M.S. and Ph.D. degrees in Physics from the Air Force Institute of Technology in 1981 and 1986. He is currently Professor of Physics at the Air Force Institute of Technology, having served as a member of the faculty since 1989. Professor Perram's research interests include chemical lasers, remote sensing, optical diagnostics, and laser weapon systems modeling.

Mr. Greg Pitz received his B.A. degree in Physics from Wright State University in 2001, and after teaching at the high-school level, returned to Wright State to complete his M.S. degree. He is currently serving as a Staff Scientist at the Air Force Institute of Technology. Pitz's research interests include chemical lasers and spectroscopy.

Capt. Brian Smith received his B.S. degree in Physics from the U.S. Air Force Academy in 1995, and his M.S. degree in Physics from the Air Force Institute of Technology in 1999. He is currently a candidate for a Ph.D. degree at the Air Force Institute of Technology.